Wood Sci Technol (2016) 50:739–757
DOI 10.1007/s00226-016-0818-0

ORIGINAL

Characterisation of wood–water relationships and transverse anatomy and their relationship to drying degrade

Adam L. Redman[1,2] · Henri Bailleres[2] · Ian Turner[1,3] · Patrick Perré[4]

Received: 29 September 2015 / Published online: 26 March 2016

Abstract Characterisation of a number of key wood properties utilising 'state of the art' tools was achieved for four commercial Australian hardwood species: *Corymbia citriodora*, *Eucalyptus pilularis, Eucalyptus marginata* and *Eucalyptus obliqua*. The wood properties were measured for input into microscopic (cellular level) and macroscopic (board level) vacuum drying models currently under development. Morphological characterisation was completed using a combination of ESEM, optical microscopy and a custom vector-based image analysis software. A clear difference in wood porosity, size, wall thickness and orientation was evident between species. Wood porosity was measured using a combination of fibre and vessel porosity. A highly sensitive microbalance and scanning laser micrometres were used to measure loss of moisture content in conjunction with directional shrinkage on micro-samples of *E. obliqua* to investigate the validity of measuring collapse-free shrinkage in very thin sections. Collapse-free shrinkage was characterised, and collapse propensity was verified when testing thicker samples. Desorption isotherms were calculated for each species using wood–water relations data generated from shrinkage experiments. Fibre geometry and wood shrinkage anisotropy were used to explain the observed difficulty in drying of the different species in terms of collapse and drying stress-related degrade.

✉ Adam L. Redman
adam.redman@daf.qld.gov.au

[1] School of Mathematical Sciences, Faculty of Science and Technology, Queensland University of Technology (QUT), 2 George Street, GPO Box 2434, Brisbane, QLD 4001, Australia

[2] Agri-Science Queensland, Department of Agriculture and Fisheries, Queensland Government, 50 Evans Road, Salisbury, QLD 4107, Australia

[3] Australian Research Council Centre of Excellence for Mathematical and Statistical Frontiers (ACEMS), Queensland University of Technology (QUT), Brisbane, Australia

[4] LGPM, CentraleSupelec, Université Paris-Saclay, Grande Voie des Vignes, 92290 Châtenay-Malabry, France

Introduction

Timber drying concerns the removal of water from wood before its end-use and consists of a complex system of intricate physical and mechanical processes. For industry, the desired outcome is to dry wood in the fastest time possible while minimising cost and maximising quality. However, due to the complexity of wood drying, these three aims are not independent; they influence each other and must be balanced to optimise the drying process. Drying time is usually restricted by the desired level of acceptable dried quality.

Dried quality includes the variation in final moisture content within and between wood boards, residual drying stress, distortion, wood cell collapse deformation, and external or internal tearing of wood tissue in the form of splits or checks. Many eucalypt species, particularly those of low density, are prone to collapse deformation, splitting and checking.

When wood dries, its exterior dries more rapidly than the interior to form a moisture content gradient. Once the exterior layers dry below the fibre saturation point, below which wood starts to shrink, and while the interior is still saturated, stresses are set up because the shrinkage of the outer layers is restricted by the wet interior (this is known as differential shrinkage). The wood tissues rupture, and consequently, splits and cracks occur if these stresses across the grain exceed the strength. Collapse describes the deformation of single cells, due to capillary forces during removal of free water, resulting in larger than normal levels of shrinkage and irregular deformation of timber surfaces. Different species are more prone to certain forms of drying-induced degrade than others depending on a number of factors mostly relating to wood anatomy, chemistry and growth conditions.

The successful control of drying defects in a drying process consists in maintaining a balance between the rate of evaporation of moisture from the surface and the rate of outward movement of moisture from the interior of the wood. One of the most successful ways of controlled wood drying is by kiln drying.

Conventional kiln drying with controlled heating, humidity and airflow under atmospheric pressure conditions is the primary method for drying timber in Australia (Nolan et al. 2003). In recent years, with emerging technological advancements in construction, design, computer control and less expensive materials, vacuum drying of hardwood timber (particularly in Europe and USA) has been proven in many applications to be a more economical alternative to drying using conventional methods, with similar or better quality outcomes (Savard et al. 2004). For this reason, the Department of Agriculture, Fisheries and Forestry (DAF) purchased a 2-m^3 research vacuum kiln.

Preliminary results from vacuum drying trials generated much interest from the Australian hardwood timber industry. In response, DAF invested in a project to establish the viability of vacuum drying technology for drying four high volume commercial Australian hardwood species with respect to drying quality, time and cost. Moreover, it was recognised that a better knowledge of the material and associated drying behaviour is required to fully optimise the vacuum drying process in the future (Perré and Turner 2007). Therefore, a component to develop a

hardwood vacuum drying model was included in the project. The full details of the modelling and simulation work will be reported in a future paper.

Currently, much modelling work has been conducted for softwood species due to its commercial importance, and relatively simple anatomical pattern (Pang 2007; Perré et al. 2007; Perré and Turner 1999a; Salin 1991). The most accurate deterministic model to date encompasses multiscale and multiphysics descriptions of drying phenomena for softwoods (Perré 2010). The proposed modelling development for the vacuum drying of hardwood species will take advantage of the existing model *TransPore* (Perré and Turner 1999a, b) used to predict the drying behaviour of softwoods and drying of other porous media, such as concrete. The complexity of the wood structure of hardwoods together with the huge variation within and between species has resulted in limited deterministic modelling work being performed to date on these species. Additionally, limited data are currently available for vacuum drying eucalypt species.

As drying models require a number of physical and mechanical parameters to operate, appropriate initial parameters have been chosen to gain a better understanding of the wood properties that explain the drying behaviour of Australian hardwood species and satisfy major requirements for a drying model. The challenge is to identify wood properties and characteristics that account for specific behaviour, such as collapse and surface/internal checking in eucalypts and related species. These phenomena are quite difficult to assess as they result from an intricate coupling between the anatomical level, and even the ultrastructural level, and the macroscopic level. Based on this premise, the following parameters were previously measured for each species as presented by Redman et al. (2011):

1. Wood anatomy characteristics, particularly wood fibre cell wall thickness and porosity (in the radial–tangential cross section);
2. Wood–water relationship on micro-samples particularly shrinkage characteristics, and
3. Permeability and diffusivity.
4. Viscoelastic nature in the tangential and radial directions using dynamic mechanical analysis (DMA).

On average, the anatomy of Australian hardwood species is made mostly of fibres and vessels, approximately 75 %. Ray and axial parenchyma cells make up the rest at approximately 15 and 10 %, respectively (Zieminska et al. 2013). The ratio of fibres to vessels, on average, for Australian hardwoods is 2:1 (Zieminska et al. 2013). The results of Redman et al. (2011) characterised wood porosity of the species of interest using only measurements of fibre properties. However, due to the substantial proportion of vessels, characterisation of the entire cross-sectional cellular morphology, including vessels, is required to accurately determine wood porosity for precise drying modelling, linkages between morphological properties and the relevant drying characteristics for each species.

Additionally, Redman et al. (2011) were unable to characterise radial and tangential shrinkages for *E. obliqua* in their study, using 1 mm thick cross-sectional samples, due to the existence of collapse shrinkage. The most widely accepted

theory of collapse occurrence was proposed by Tiemann (1941), who attributed collapse to the hydrostatic tensions in the fibre cell lumina caused by water removal. Essentially, when drying above the fibre saturation point, free capillary water in the cell lumina is withdrawn through small cell wall openings (pits) forming a meniscus at the air–water interface, thus inducing a hydrostatic tension. If this hydrostatic tension exceeds the compressive strength of the cell wall, the cell collapses. Kauman (1965) postulates that thin cross sections, thinner than the minimum fibre length, do not collapse since each fibre has been severed and tensions cannot develop. The average fibre length for *E. obliqua* is reportedly 1.15 mm, ranging from 1.04 to 1.27 mm (Dadswell 1972), measured on 20 heartwood samples. The existence of collapse shrinkage in 1 mm thick samples observed by Redman et al. (2011) suggests that the minimum fibre length was less than the minimum reported by Dadswell (1972), the measurement of which was outside the scope of this work.

Based on previous findings and postulations, the following parameters were measured for each species and are presented in this paper:

1. Wood anatomy characteristics, particularly porosity as a combination of fibre and vessel porosity, using a combination of ESEM (environmental scanning electron microscope) scans and image analysis using *MeshPore*, which is a vector-based software package developed by Perré (2005) to characterise cell morphology and;
2. Wood–water relationship on thin sections of *E. obliqua* micro-samples (less than 1 mm) with the aim of characterising 'collapse free' shrinkage, using a highly accurate microbalance and scanning laser micrometres to accurately measure loss of moisture content (MC) in conjunction with directional shrinkage.

Wood–water relationship measurements also allow the calculation of sorption/desorption curves, the mathematical description of which is used in modelling. The sorption hysteresis effect, i.e. different wood equilibrium moisture content (EMCs) in desorption and adsorption for the same relative humidity, is well known (Skaar 1988). However, quantitative sorption isotherms in the form of tables or analytical correlations are usually given as the average of the desorption and adsorption curves. Consequently, most drying simulation models use these average curves and do not take into account the sorption hysteresis phenomenon (Salin 2011).

Salin (2011) proposed that traditional models which use average sorption curves (derived across a range of species) are problematic because different species have different sorption isotherms. Therefore, species specific sorption isotherms, including the sorption hysteresis phenomenon, of which drying models are very sensitive, should be included in drying models as an improved tool in practical applications. For this reason, in this paper sorption isotherms are presented which were calculated from the results of Redman et al. (2011) for *Corymbia citriodora* Hook. (spotted gum), *Eucalyptus pilularis* Sm. (blackbutt) and *Eucalyptus marginata*, D.Don ex Sm. (jarrah) and from the results of this paper for *Eucalyptus obliqua* L'Herit. (messmate).

These species were chosen for this study based on their large commercial volume, value and range of drying characteristics and wood properties. For example, *C. citriodora* is the easiest species to dry in terms of resistance to drying degrade and has the highest basic density (BD) of 1000 kg/m^3 (Bootle 2005), followed by *E. pilularis* (710 kg/m^3 BD) and *E. marginata* (670 kg/m^3 BD), which are mildly susceptible to surface checking. Finally, *E. obliqua* is one of the Australia's hardest species to dry due to its propensity to collapse, internal and surface check and has the lowest BD of 489 kg/m^3. The basis of this study consists of accurately quantifying a number of morphological and wood–water relation variables necessary to develop a precise deterministic hardwood vacuum drying model using the aforementioned species as case studies. Additionally, linkages between these and previously measured properties and the susceptibility for drying-induced degrade to occur between the species are observed.

Materials and methods

Material for this study was selected from concurrent vacuum drying studies. These trials indicated that for any given species, the median density board most closely aligned to the average drying rate during a drying trial (Redman 2011). Thus, for each species, the board having the median basic density was selected from a quantity of 100 samples to perform morphological characterisation and investigate wood–water relations. Figure 1 shows an example of the typical normal (calculated using the Shapiro–Wilk test) density distribution histogram for *Eucalyptus obliqua*.

Morphological characterisation

For each species, fibre morphology was captured using an FEI Quanta 200 ESEM microscope with a beam voltage of 12.2 kV and vacuum pressure of 12 mbar. Vessel morphology was captured using a Zeiss Axioplan stereo optical microscope, using transmitted light, fitted with a monochrome digital camera.

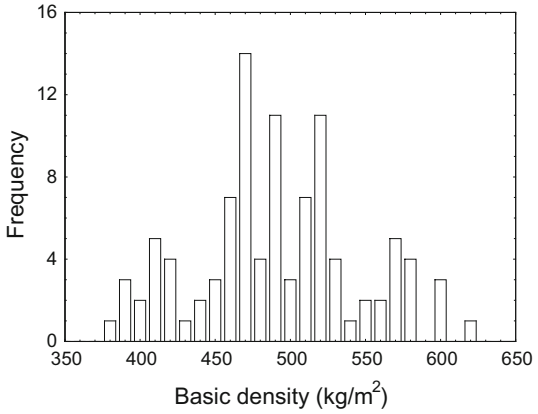

Fig. 1 Density distribution histogram example for *Eucalyptus obliqua*

Small heartwood samples were cut from unseasoned boards. One sample per species was carefully cut using a laboratory bandsaw to the approximate dimensions: 4 mm (radial) × 4 mm (tangential) × 20 mm (longitudinal). The samples were cut in half lengthwise to produce two matched samples of dimension: 4 mm × 4 mm × 10 mm. Samples were soaked in water at room temperature for at least 24 h, before further processing, to soften the wood tissue prior to image surface preparation. Radial/tangential plane surfaces were prepared for ESEM imaging using a precision MICROM HM 440^{TM} sledge/sliding microtome. One section was used for microscopic analysis in the radial–tangential plane, while the other section was used to determine basic density. One image was analysed per species. It should be noted that the earlywood and latewood variation is not high in these species and they are all diffuse porous.

Images taken at 700× magnification were used for measurement of fibre properties (Fig. 2), and images taken at 50× magnification were used for measurement of vessel properties (Fig. 3) using *MeshPore* (Perré 2005). The fibre ESEM images were cropped to contain only wood fibres excluding ray parenchyma and vessel cells. *MeshPore* is a stand-alone application allowing a comprehensive finite element (FE) mesh to be prepared from digital microscopic images of heterogeneous and porous media, and fast measurements of the wood morphology can also be calculated. Using *MeshPore*, fibre and vessel lumen contours were automatically generated (Fig. 4) to determine the average fibre cell wall thickness, fibre, vessel and total porosities.

The average fibre cell wall thickness (μm) was calculated by *MeshPore* using Eq. 1:

$$t_{\mathrm{f}} = \frac{A_i - \sum_{j=1}^{n} A_j}{\sum_{j=1}^{n} l_j}, \tag{1}$$

where t_{f} is the average fibre thickness, A_i is the area of the fibre image (m^2), A_j is the fibre void area (m^2) of void number j, n is the number of voids in the image and l_j is the fibre void circumference of void number j.

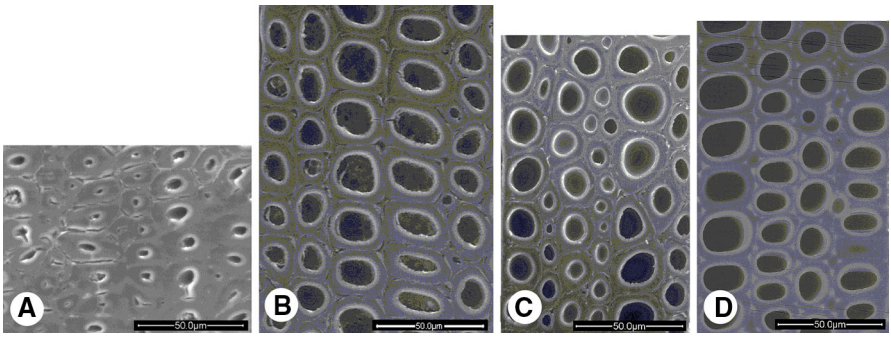

Fig. 2 Cropped ESEM images for fibre morphology analysis: *C. citriodora* (**a**), *E. marginata* (**b**), *E. pilularis* (**c**) and *E. obliqua* (**d**)

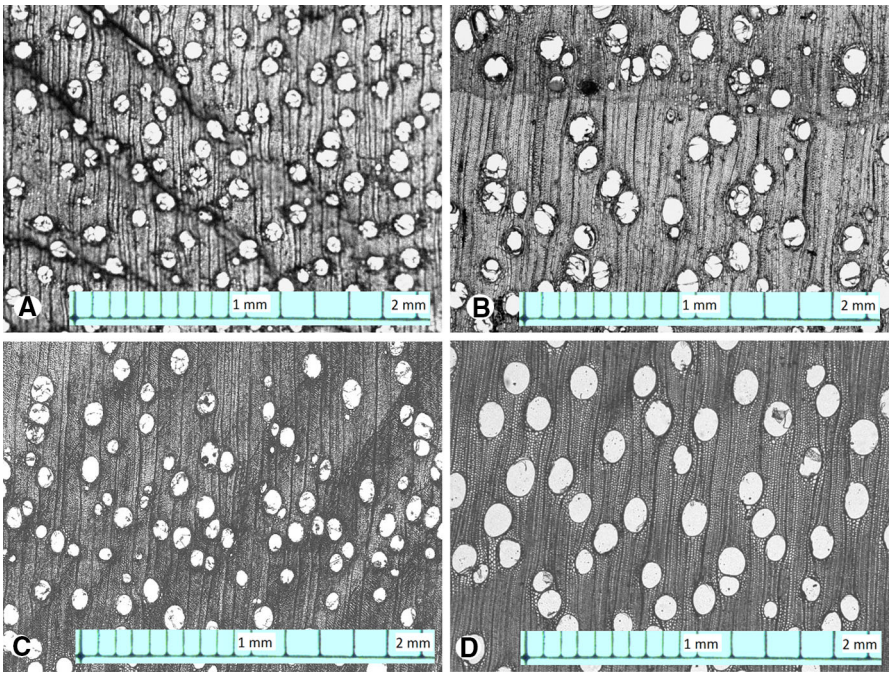

Fig. 3 Optical microscope images for vessel morphology analysis: *C. citriodora* (**a**), *E. marginata* (**b**), *E. pilularis* (**c**) and *E. obliqua* (**d**)

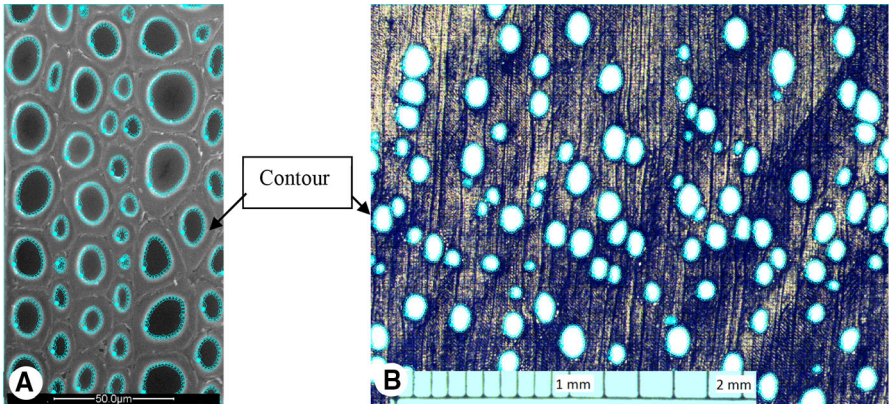

Fig. 4 Example of automated *MeshPore* contours generated for *E. pilularis* fibres (**a**) and vessels (**b**)

Equation (1) assumes that the surface fraction of the solid phase is equal to the averaged cell wall thickness multiplied by the total contour length. As the cell walls have a closed contour rather than being flat, the exact formula should use an averaged contour, somewhere between the lumen contour and the contour of the middle lamella. Using the lumen contour is simpler and more reproducible.

However, it has to be kept in mind that the error due to this simple formula is negligible only when the cell wall thickness is small compared to the lumen diameter.

The fibre or vessel porosities (%) were calculated by *MeshPore* using Eq. 2:

$$\varphi_x = \frac{\sum_{j=1}^{n} A_{jx}}{A_i} \times 100 \tag{2}$$

where x represents either fibres (f) or vessels (v), and φ_x is the porosity (%). For such a dual-scale porous structure, the total porosity was calculated as the vessel porosity plus the fibre porosity inside the remaining volume using Eq. 3:

$$\varphi_{\mathrm{t}} = \varphi_{\mathrm{f}} + (1 - \varphi_{\mathrm{f}})\varphi_{\mathrm{v}} \tag{3}$$

The density was calculated using total porosity to determine whether density can be predicted using only this parameter. The formula uses the oven-dried density of wood tissue, assumed constant for all wood species, the value of which is reported to be approximately 1500 kg/m^3 (Siau 1984). Equation 4 was used to calculate density:

$$\rho_{\mathrm{calc}} = \rho_{\mathrm{wt}}(1 - \varphi_{\mathrm{t}}) \tag{4}$$

where ρ_{calc} is the calculated density and ρ_{wt} is the density of wood tissue (1500 kg/m^3).

Wood–water relations

Wood–water relationship tests were carried out on 2, 1 and 0.5 mm longitudinally thick micro-samples of *E. obliqua* using specialised precision apparatus (Perré 2007). Such thin samples, prepared using a precision diamond wire saw, are used to produce a relatively uniform MC field, thus minimising the stress field so as not to produce checks or cracks during testing. As already stated, such small thicknesses are also needed to avoid, or at least reduce, collapse.

During testing, the dimensions of micro-samples were measured using a noncontact laser system while continuously measuring the MC of samples using a highly sensitive electronic microbalance (MC2, Sartorius) with a capacity of 2 g and typical sensitivity of 0.1 µg. Two high-speed laser micrometres (Keyence, LS-5000 series) were incorporated to measure changes in the width and height of samples without contact (2 µm accuracy and 0.3 µm reproducibility).

The measurement system was placed in a climatic chamber where the dry bulb temperature was held constant at 30 °C. Relative humidity inside the chamber was controlled using a water bath maintained at the desired dew point temperature. A small fan ensured even temperature and humidity conditions throughout the chamber. Using a dew point analyser, the actual dew point of the chamber was checked to correspond to the water temperature to an accuracy of 0.1 °C (Perré 2007).

A small block of unseasoned material was initially prepared with the approximate dimensions: 13 mm in the tangential (T) direction, 10 mm in the

radial (R) direction and 40 mm in the longitudinal direction (L). The block was then sliced in the longitudinal direction using a diamond wire saw to accurately obtain radial/tangential cross-sectional samples of the required thickness.

Prior to testing, samples were inserted into a sample support specifically designed so (refer to Perré 2007 for further detail):

- It does not interfere with the laser beams,
- Shrinkage measurements are made at the same material locations, and
- The sample is sufficiently restrained to avoid flexure while maintaining freedom to shrink (Fig. 5).

Radial and tangential shrinkages were investigated on two samples for each sample thickness (2, 1 and 0.5 mm). For each test, the dew point temperature was cycled as shown in Fig. 6. The corresponding relative humidity in the chamber is also depicted in this graph.

During each test, shrinkage, temperature and sample weight measurements were recorded at regular intervals and stored. At the end of the experiment, the sample was oven-dried to determine the final MC of the sample and previous MC evolution during the test.

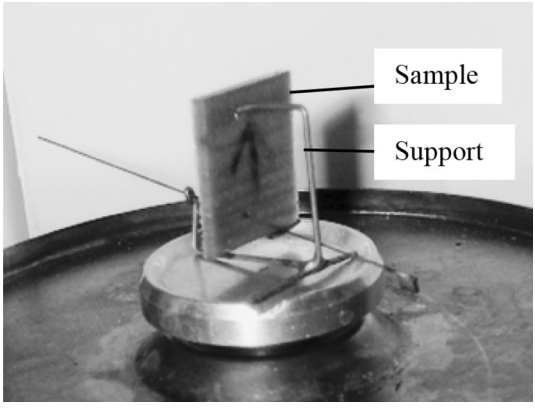

Fig. 5 Sample in support resting on microbalance

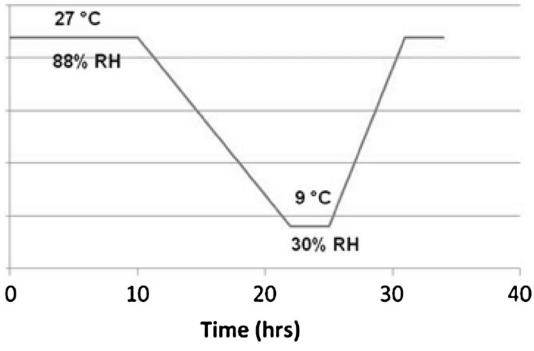

Fig. 6 Climatic schedule used for shrinkage tests

Investigations of sample MC versus surrounding relative humidity (RH) were conducted to observe the sorption/desorption characteristics and hysteresis for each species. Based on previous work conducted by Perré (2007), the tests reported here are considered to be quasi-static in the desorption and adsorption phases. The length of time between each test set point (Fig. 6) combined with the thin sample sections is sufficient for the system to remain close to internal equilibrium to provide an approximation of a true desorption/sorption isotherm. Then, Eq. (5) is fitted to the desorption/sorption data in the least-squares sense by solving for c_1 and c_2 as reported by Perré and Turner (2008):

$$\frac{P_v}{P_{vs}} = 1 - \exp(-c_1 A - c_2 A^2) \text{ and } A = X_b/X_{fsp}, \quad (5)$$

where c_1 and c_2 are constants, P_v is the vapour pressure of air (P_a), P_{vs} is the saturated vapour pressure of air, X_b is the wood MC (%) and X_{fsp} is the MC (%) at fibre saturation point (FSP). As the desorption phase is more applicable to wood drying, desorption RH and MC data were used to obtain the constants c_1 and c_2 for 0.5 mm thick *E. obliqua* samples and 1 mm thick samples for the other species. Thinner *E. obliqua* samples were used to minimise error caused by collapse shrinkage. The values c_1 and c_2 are essential species-dependent constant properties that are required for the development of an accurate wood drying model.

Results and discussion

Morphological characterisation

Table 1 contains the number of fibres and vessels measured, average fibre cell wall thickness, fibre, vessel and calculated total porosity, and measured and calculated density for each species. As the calculated cell wall thickness using *MeshPore* is based on the global sum of contours and tissue area, individual values are not calculated, which prevents standard deviations to be determined.

Distinct fibre and vessel porosity and fibre cell wall thickness differences between species were measured, as visually observed from ESEM images. Fibre cell wall thickness results (from 3.6 to 6.1 μm depending on species) are consistent with

Table 1 Average cell wall thickness (using *MeshPore*), fibre, vessel and total porosity, and measured and calculated densities for each species in the unseasoned condition ($n = 1$)

Species	No. fibres	No. vessels	Fibre cell wall thickness (μm)	Fibre porosity (%)	Vessel porosity (%)	Total porosity (%)	Measured basic density (kg/m^3)	Calculated density (kg/m^3)
C. citriodora	56	125	6.1	7	16	22	921	1172
E. marginata	82	80	3.9	26	17	38	636	927
E. pilularis	113	113	4.1	28	14	38	674	927
E. obliqua	95	59	3.6	37	19	49	489	765

published data (Ressel 2008), which suggests the average fibre cell wall thickness for wood generally ranges from around 3 to 8 μm. *C. citriodora* has the lowest fibre, vessel and hence total calculated porosity and *E. obliqua* the highest.

The calculated species density decreases with fibre cell wall thickness and increasing total porosity. Although fibre cell wall thickness and porosity play important roles in the overall density of wood, the frequency and cell wall thickness of ray parenchyma cells, and the frequency and size of hardwood vessels also contribute (Ressel 2008).

Calculated density values are always higher than the basic density measured on the samples used to grab ESEM images. The major reason for this systematic bias is that basic density, the oven-dry mass divided by the saturated volume, is the smallest value which can be obtained, whereas the calculated values use the published oven-dry density of wood tissue and the cell geometry determined on the sample in the ESEM chamber, at an equilibrium moisture content close to dry state. Another reason for this difference is due to the fact that the current image analysis study focused on fibres and vessels. Other tissues of smaller density were not taken into consideration such as axial and ray parenchyma, which make up approximately 25 % of wood tissue volume (Zieminska et al. 2013). Additionally, intra-wall voids could also contribute to a lesser extent. However, a strong correlation was observed between measured and calculated densities ($R^2 = 0.99$).

Wood–water relations

For *E. obliqua* at 2, 1 and 0.5 mm sample thicknesses, tangential and radial shrinkages versus MC curves were plotted as illustrated in Fig. 7a, b. Note that the data define a very accurate curve during the test period as the adsorption/desorption shrinkage closely follows the same curve (low MC tail of the graph). This feature has already been observed and previously reported (Almeida et al. 2009; Perré 2007): depending on the moisture history, the sorption hysteresis changes the equilibrium content for a given relative humidity, but the sample dimensions depend only on the sample moisture content. The curves include two different phases:

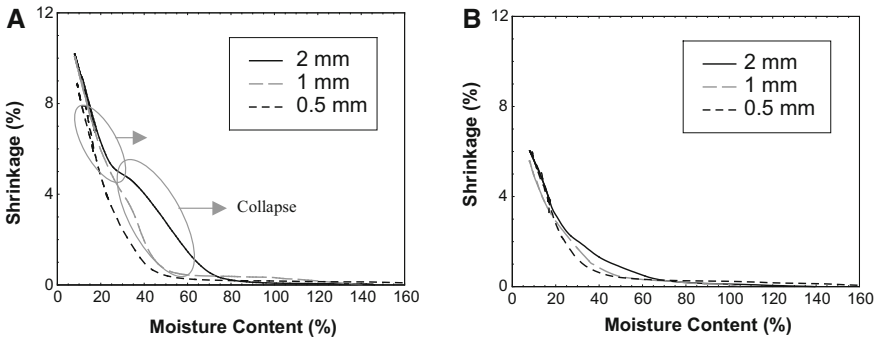

Fig. 7 *E. obliqua* tangential shrinkage curves showing collapse (**a**) and radial shrinkage curves (**b**) for 2, 1 and 0.5 mm thick samples

- the removal of free water with minimal shrinkage, and
- a noticeable shrinkage phase, denoting the removal of bound water with a linear relationship with MC.

However, for 2 and 1 mm thick samples abnormal shrinkage is present occurring at high MC due to cell collapse during free water removal. This is more evident in the tangential direction as shown in Fig. 7a. It appears that collapse shrinkage is eliminated by testing using 0.5 mm thick samples. Dadswell (1972) measured the fibre length of 20 *E. obliqua* specimens; the results ranging from a length of 1.04–1.27 mm. Thus, by reducing the dimension of the sample to less than 1 mm thickness, the majority of wood fibres should be severed. As tension of water inside the lumen is due to the huge percolation pressure required for air to go through the pits, a cut fibre will not collapse (Redman et al. 2011).

The fibre saturation point (FSP) is in many applications assumed as the MC below which specific wood properties begin to change as a function of MC. Several methods exist to measure FSP. In the work presented here FSP is calculated by the shrinkage intersection point (SIP). This method assumes that no collapse occurs during the removal of liquid water. As this method is valid only in the absence of shrinkage, the thinner (0.5 mm thick) samples were used for this purpose. This is simply done from the shrinkage versus MC curves by subtending the linear portion of the curve, in the bound water/shrinkage phase, until it intersects the x and y axes (Fig. 8). The shrinkage at 12 %, a common published quantification of shrinkage, was calculated from the equation of the subtended line (slope). Table 2 provides the total shrinkage, FSP, shrinkage at 12 %, and the radial/tangential (R/T) shrinkage ratios of the 0.5-mm-thick *E. obliqua* samples along with previously published data for *E. marginata*, *E. pilularis* and *C. citriodora* for comparison (Redman et al. 2011). Published 12 % MC shrinkage values (Bootle 2005) are also included.

Published FSP and 12 % MC shrinkage values are consistent with measured data. It is interesting to note that the trend of increasing FSP values recorded aligns with increasing drying difficulty per species. That is, in this case, species with a higher

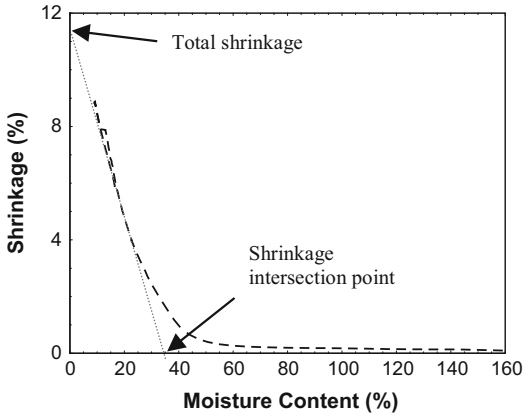

Fig. 8 Example of total shrinkage and shrinkage intersection point (FSP) determination

Table 2 Shrinkage data measured for 0.5 mm thick *E. obliqua* samples compared with previously measured data (Redman et al. 2011)

Sample #	Species	Intersection point (FSP) MC (%)		Total shrinkage (%)		Shrinkage at 12 % MC					
						Measured			Bootle (2005)		
		R	*T*	*R*	*T*	*R*	*T*	*R/T*	*R*	*T*	*R/T*
1	*E. obliqua*	28.0	31.3	9.0	12.3	5.0	7.6	0.66	3.5	6.5	0.54
3	*E. obliqua*	28.1	33.5	8.0	11.7	4.7	7.5	0.63			
1	*E. marginata*	29.0	34.7	8.2	11.9	4.8	7.8	0.62	5.0	7.5	0.67
2	*E. marginata*	26.0	34.6	8.4	13.4	4.7	8.9	0.53			
1	*E. pilularis*	24.5	31.8	8.5	12.6	4.5	7.9	0.57	4.0	7.0	0.57
2	*E. pilularis*	25.2	30.6	8.4	12.1	4.4	7.3	0.60			
1	*C. citriodora*	23.6	25.9	8.6	8.8	4.4	4.9	0.90	4.5	6.0	0.75
3	*C. citriodora*	24.5	23.0	8.3	8.6	4.5	5.2	0.87			

FSP are more prone to checking collapse and splitting during drying. Shrinkage values and *R*/*T* ratios vary greatly between the tangential and radial directions, except for *C. citriodora* where the ratio is closer to 1:1. This may contribute to the relative resistance of this species to drying related mechanical defect in conjunction with low FSP values, compared to the other species.

By observing the MC versus RH sorption/desorption curves for each species, the hysteresis phenomenon is evident (Fig. 9). The curves differ for each species due to different anatomical and chemical composition. In particular, extractive content levels and composition heavily influence sorption/desorption behaviour, where the removal of extractives leads to higher equilibrium moisture content at a given relative humidity (Bibiak 2007). The reducing RH/MC part of the curve (top part) is the desorption curve and is more applicable to wood drying, which is a desorption process. Using data from this part of the curve, the constants c_1 and c_2 were calculated in the least-squares sense using Eq. (5) for each species and are presented

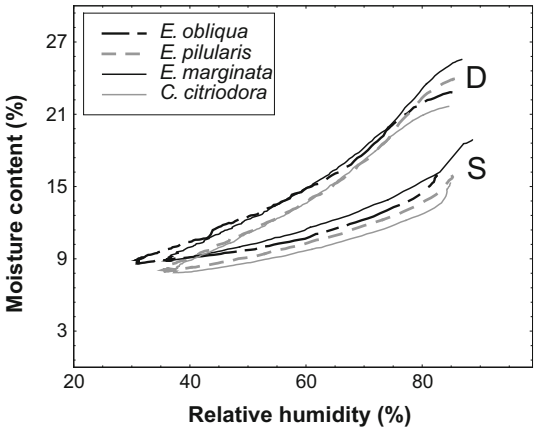

Fig. 9 Desorption (D)/sorption (S) curves for each species

Table 3 Desorption isotherm solutions for constants c_1 and c_2

Species	c_1	c_2
E. obliqua	0.808	2.2796
E. marginata	0.9716	0.8401
E. pilularis	1.1847	0.7211
C. citriodora	1.0047	0.9076

in Table 3. The values presented are generally consistent between species except for *E. obliqua* where the value of the c_2 parameter is more than double that computed for the other species. Further investigation reveals that an increase in parameter c_2 results in a higher sorption/desorption MC for a given RH. This is evident in the sorption/desorption curve. A higher isotherm MC for a given RH also results from a higher shrinkage intersection MC. This is evident for the isotherm curves of species *E. obliqua* and *E. marginata,* which recorded the highest intersection MC values.

From anatomical and physical properties to drying degrade

As stated in the introduction, this work aims at reporting a comprehensive study of some Australian species for drying application purposes. It is therefore very interesting to check whether or not the data collected at a microscopic scale (anatomical observations and measurements on minute samples) can help with the understanding and the control of industrial drying. A further analysis of the whole dataset is proposed here and compared to drying trials performed in a 2-m^3 laboratory kiln.

Wood species susceptibility to different types of drying degrade can be attributed to a number of physical, mechanical and environmental properties. Wood fibre collapse has been found to increase with temperature (Innes 1996; Kauman 1965), and also be affected by species, age, climate (Guernsey 1951; Kauman 1965), density (Chafe 1985), tree position (Cuevas 1969; Pankevicius 1961), growth rings (Bisset and Ellwood 1950), chemical and cell structure (Kauman 1965). Kauman (1965) states that collapse depends on the cell pore size, thickness and strength where small variations can cause large variations on collapse intensity. He states that correlation of collapse with any anatomical feature will be at least partly obscured by random statistical variations in these properties.

The propensity for stress-related drying degrade, such as end-splitting, and surface and internal checking, can be exacerbated by low diffusion rates and high shrinkage (Perré and Wieslaw 2007). Additionally, collapse degrade has also been shown to intensify and/or initiate internal checking (Innes 1996). Drying stress-related splitting and checking (external and internal) can be reduced by the presence of interlocked grain (Harris 1989).

Qualitative and quantitative data used to investigate the drying behaviour are provided in Table 4. They include the fibre lumen diameter, fibre cell wall thickness and their ratio, the ratio of total radial to tangential shrinkage (calculated from Table 2), and the ratio of transverse total shrinkage to diffusion coefficient. Diffusion coefficient values were previously published by Redman et al. (2011).

Table 4 Quantitative and qualitative data for comparison between drying degrade propensity

Species	Fibre lumen diameter (μm)	Fibre cell wall thickness (μm)	Fibre cell wall diameter: thickness ratio	Total shrinkage R:T ratio	Transverse shrinkage: diffusion coefficient ratio	Collapse shrinkage observed	Splitting/ checking propensity	Grain type
C. citriodora	4.0	6.1	0.66	0.98	6.09E+11	No	Low	Interlocked
E. marginata	12.0	3.9	3.08	0.65	4.92E+11	No	Low	Interlocked
E. pilularis	9.3	4.1	2.27	0.69	4.64E+11	No	High	Straight/slightly interlocked
E. obliqua	11.7	3.6	3.26	0.71	2.10E+11	Yes	High	Straight

Table 5 Example of drying degrade results from industry drying trials

Species	Percentage of boards affected[a]			
	Collapse	Surface check	Internal check	End-split
C. citriodora	0	17	0	11
E. marginata	0	16	12	6
E. pilularis	0	83	0	64
E. obliqua	100	29	4	77

[a] $n = 100$

Drying degrade, observed from a series of drying trials (Redman 2011), includes the species propensity to collapse, split and check, and the species grain type: interlocked, straight or a combination. Quantitatively, the percentage of collapse, surface check, internal check and end-split of 100 boards dried in industrial drying trials (Redman 2011) are provided in Table 5.

Instead of trying a multifactorial analysis of all these parameters, some synthetic indicators built from the database were derived that are likely to explain the drying behaviour:

1. *The propensity to collapse*: as it is almost impossible to obtain reliable information regarding the percolation pressure, analysis was limited to the ability of cells to withstand negative pressure. A simple analysis of stress in a cylinder tells us that the ratio of lumen diameter over cell wall thickness is a relevant parameter.
2. *The propensity for deformation*: the shrinkage ratio is well known to be involved in the deformation of sections due to bound water removal. A very anisotropic shrinkage may also induce drying stresses due to incompatible strain fields.
3. *The propensity to induce drying stress*: drying stresses are produced during drying due to the nonuniform strain field generated by shrinkage. This strain heterogeneity obviously increases with the shrinkage value and the extent of the moisture gradient profile. Therefore, the shrinkage value along the board surface divided by the mass diffusivity along the normal is a good candidate.

Figure 10a plots the ratio of fibre lumen to cell wall thickness versus indicator 2 (total radial/tangential shrinkage ratio) for each species. The plot shows *E. obliqua* exhibits the highest tendency to collapse compared with other species, a fact backed up by experimental data (Table 5). The plot also indicates *E. marginata* and *E. pilularis* may be prone to collapse. Although not observed in experimental data, published data confirm that *E. pilularis* at least is prone to collapse (Raymond et al. 2008). In terms of both fibre properties and its almost 1:1 radial/tangential shrinkage ratio, *C. citriodora* exhibits low collapse and drying stress degrade propensity compared with the other species. The other species are shown to be collectively more prone to deformation-related degrade (Fig. 10a; Table 5).

Figure 10b provides another observation of the relationship between species: the propensity to drying stress (indicator 3) versus the collapse propensity (indicator 1).

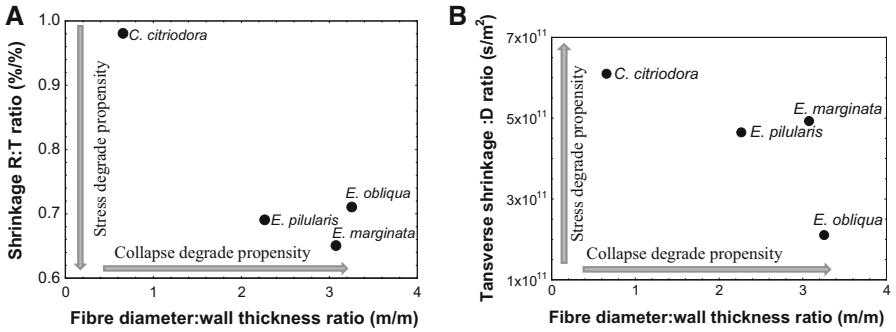

Fig. 10 Species propensity to deform and stress drying degrade based on fibre geometry ratio and **a** transverse shrinkage ratio and **b** transverse shrinkage to diffusion ratio 3

The same collapse propensity relationship is evident as for Fig. 10a; however, these results indicate that *C. citriodora* should be comparatively more prone to stress-related degrade. This does not agree with the measured data (Table 5). This discrepancy is likely due to the very tight interlocked grain of *C. citriodora,* which can provide more resistance to drying stress wood tissue rupture compared with the straight grain of *E. obliqua*. Additionally, *E. obliqua* is possibly more prone to checking due to its propensity (100 % for this species and 0 % for others) to collapse (a factor not included in this analysis). Further research into the effect of interlocked grain on drying degrade is recommended.

Conclusion

Cell wall thickness and wood porosity as a combination of fibre and vessel porosity, using a combination of ESEM and optical microscope scans, and image analysis using *MeshPore* were realised for each species. Clear differences in these values between species were evident. A strong correlation exists between measured and calculated wood density based on porosity measurements. Higher calculated values were evident as they do not take into account axial and ray parenchyma cell and intra-wall voids. Measurement of radial and tangential shrinkages for *E. obliqua* using a highly accurate, dynamic method free of collapse shrinkage was achieved and was consistent with published data. This was not possible in a previous study by Redman et al. (2011) that used relatively thick samples, but was accomplished using very thin 0.5 mm samples. Thicker samples were also tested in this study to demonstrate their propensity to collapse. Data obtained from the shrinkage measurements of *E. obliqua* from this study and *C. citriodora*, *E. pilularis* and *E. marginata* from the previous study by Redman et al. (2011) allowed the generation of sorption/desorption curves for each species. Data were used to approximate desorption isotherms for each species with the *E. obliqua* results substantially different to the other species. As previously reported *E. obliqua* exhibits properties that are generally extreme or do not follow the typical trend when compared to other

species. *Eucalyptus obliqua* is by far the hardest wood to dry in terms of collapse and checking and also exhibits more extreme wood properties compared to easier to dry species.

Accurate determination of wood porosity, tangential and radial shrinkages, and desorption isotherms are parameters necessary for precise deterministic modelling of the drying process.

These results indicate that by comparing certain data related to drying degrade, it is possible to explain the observed difficulty in drying relevant to different species. Fibre geometry can be used to provide an indication of collapse propensity and the ratio of total radial: tangential shrinkage may be linked to stress degrade propensity. Care must be taken, however, as other wood characteristics and properties may need to be considered such as the presence of interlocked grain.

Acknowledgments The substantial contributions of AgroParisTech Nancy, Queensland University of Technology (QUT), Forest and Wood Products Australia (FWPA) and the Queensland Government Department of Agriculture and Fisheries (DAF), to the successful undertaking of this collaborative project are gratefully acknowledged.

References

Almeida G, Brito JO, Perre P (2009) Changes in wood–water relationship due to heat treatment assessed on micro-samples of three *Eucalyptus* species. Holzforchung 63:80–88

Bibiak M (2007) Chapter 4—Sorption isotherms of wood. In: Perré P (ed) Fundamentals of wood drying. A.R.BO.LOR, Nancy, pp 87–104

Bisset IJW, Ellwood EL (1950) The relation of differential collapse and shrinkage to wood anatomy in *Eucalyptus regnans* F.v.M. and *E. gigantea* Hook F. Aust J Appl Sci 2:175–183

Bootle KR (2005) Wood in Australia—types, properties and uses, 2nd edn. McGraw Hill, Sydney

Chafe SC (1985) The distribution and interrelationship of collapse, volumetric shrinkage, moisture content and density in trees of *Eucalyptus regnans* F. Muell. Wood Sci Technol 19:329–345

Cuevas LE (1969) Shrinkage and collapse studies on *Eucalyptus viminalis*. J Inst Wood Sci 23:29–38

Dadswell HE (1972) The anatomy of eucalypt woods. Commonwealth Scientific and Industrial Research Organisation, Melbourne

Guernsey FW (1951) Collapse in western red cedar. Br Columbia Lumberm 4:3

Harris JM (1989) Spiral grain and wave phenomena in wood formation. Springer, Berlin

Innes TC (1996) Collapse and internal checking in the latewood of *Eucalyptus regnans* F. Muell. Wood Sci Technol 30:373–383

Kauman WG (1965) Cell collapse in wood. CSIRO-Division of Forest Products, Melbourne

Nolan G, Innes TC, Redman AL, McGavin R (2003) Australian hardwood drying best practice manual. Forest and Wood Products Research and Development Corporation. www.fwpa.com.au

Pang S (2007) Mathematical modeling of kiln drying of softwood timber: model development, validation and practical application. Dry Technol 25:421–431

Pankevicius ER (1961) Influence of position in tree on recoverable collapse in wood. For Prod J 11:131–132

Perré P (2005) Meshpore: a software able to apply image-based meshing techniques to anisotropic and heterogeneous porous media. Dry Technol 23:1993–2006

Perré P (2007) Experimental device for the accurate determination of wood–water relations on micro-samples. Holzforschung 61:419–429

Perré P (2010) Multiscale modeling of drying as a powerful extension of the macroscopic approach: application to solid wood and biomass processing. Dry Technol 28:944–959

Perré P, Turner IW (1999a) A 3-D version of TransPore: a comprehensive heat and mass transfer computational model for simulating the drying of porous media. Int J Heat Mass Transf 42:4501–4521

Perré P, Turner IW (1999b) Transpore: a generic heat and mass transfer computational model for understanding and visualising the drying of porous media. Dry Technol 17:1273–1289
Perré P, Turner I (2007) Chapter 10—Coupled heat and mass transfer. In: Perré P (ed) Fundamentals of wood drying. A.R.BO.LOR, Nancy, pp 203–241
Perré P, Turner IW (2008) A mesoscopic drying model applied to the growth rings of softwood: mesh generation and simulation results. Maderas, Ciencia y technologia 10:251–274
Perré P, Wieslaw O (2007) Chapter1—From fundamentals to practice the interaction chain. In: Perré P (ed) Fundamentals of wood drying. A.R.BO.LOR, Nancy, pp 1–9
Perré P, Rémond R, Aléon D (2007) Energy saving in industrial wood drying addressed by a multiscale computational model: board, stack, and kiln. Dry Technol 25:75–84
Raymond CA et al (2008) Improving dimensional stability in plantation-grown *Eucalyptus pilularis* and *E. dunii*. www.fwpa.com.au
Redman AL (2011) Evaluation of super-heated steam vacuum drying viability and development of a predictive drying model for Australian hardwood species. Queensland Government Department of Employment, Economic Development and Innovation report for Forestry and Wood Products Australia. www.fwpa.com.au
Redman AL, Bailleres H, Perré P (2011) Characterization of viscoelastic, shrinkage and transverse anatomy properties of four Australian hardwood species. Wood Mat Sci Eng 6:95–104
Ressel JB (2008) Wood anatomy—an introduction. In: Perre P (ed) Fundamentals of wood drying. A.R.BO.LOR ENGREF, Nancy, p 19
Salin JG (1991) Modeling of wood drying: a bibliography. Dry Technol 9:775–793
Salin JG (2011) Inclusion of the sorption hysteresis phenomenon in future drying models. Some basic considerations. Maderas Ciencia y tecnologia 13:173–182
Savard M, Lavoie V, Trembala C (2004) Technical and economical assessment of superheated steam vacuum drying of Northern Red Oak. In: N.A.G.R.E.F. COST E15 conference, Athens, Greece, 22–24 April 2004, Forintek Canada Corp., pp 1–10
Siau JF (1984) Transport processes in wood. Springer, Berlin
Skaar C (1988) Wood–water relations. Springer, Berlin
Tiemann HD (1941) Collapse in wood as shown through the microscope. J For Res 39:271–282
Zieminska K, Butler DW, Gleason SM, Wright IJ, Westoby M (2013) Fibre wall and lumen fractions drive wood density variation across 24 Australian angiosperms. AoB Plants 5:14